A Microgrid Based on Wind Driven DFIG, DG and Solar PV Array for Optimal Fuel Consumption

Sambasivaiah Puchalapalli, *Member, IEEE,* S.K. Tiwari, Bhim Singh, *Fellow, IEEE*, and P.K. Goel

***Abstract*—This paper presents a green energy solution to a microgrid for a location dependent on a diesel generator (DG) to meet its electricity requirement. This microgrid is powered by two renewable energy sources namely wind energy using doubly fed induction generator (DFIG) and solar photovoltaic (PV) array. The solar PV array is directly connected to common DC bus of back-back voltage source converters (VSCs), which are connected in the rotor side of DFIG. Moreover, a battery energy storage (BES) is connected at same DC bus through a bidirectional buck/boost DC-DC converter to provide path for excess stator power of DFIG. The extraction of maximum power from both wind and solar, is achieved through rotor side VSC control and bidirectional buck/boost DC-DC converter control, respectively. A modified perturb and observe (P&O) algorithm is presented to extract maximum power from a solar PV array. Moreover, the control of load side VSC, is designed to optimize the fuel consumption of DG. A novel generalized concept is used to compute the reference DG power output for optimal fuel consumption. The microgrid is modelled and simulated using SimPowerSystems tool box of MATLAB, for various scenarios such as varying wind speeds, varying insolation, effect of load variation on a bidirectional converter and unbalanced nonlinear load connected at point of common coupling (PCC). The DFIG stator currents and DG currents, are found balanced and sinusoidal. Finally, a prototype is developed in the laboratory to validate the design and control of it.**

***Index Terms*—Wind Turbine, doubly fed induction generator (DFIG), diesel generator, solar photovoltaic array, bidirectional buck/boost DC-DC converter, battery energy storage, power quality.**

I. INTRODUCTION

Diesel generators (DGs) are very popular for the decentralized power generation as well as backup power in the urban housing society for the following reasons [1]-[3].

- DGs are portable and dispatchable.
- They are of lower capital cost.
- DGs maintenance is easier.
- They have higher conversion efficiency as compared to other sources of energy resulting in low specific greenhouse gas emission.

For the above reasons, they are widely used for the power distribution of islands, commercial and military ships etc [4]. However, DGs suffer from the higher running cost along with noise and air pollution. The running cost is dependent on amount of fuel consumption based on the power generation. This cost is minimized by installing renewable energy (RE) sources such as wind, solar and biomass etc. Moreover, RE based power sources are pollution free and abundant in nature. Among RE sources, wind and solar are considered to be more popular because of their reduced cost and technological advancements [5], [6]. Wind turbines are mainly categorized as fixed speed and variable speed type. Fixed speed wind turbines have been used earlier due to their simple operating features. However, they suffer with more power loss. Variable speed wind turbines with doubly fed induction generator (DFIG), are dominantly used for wind energy extraction due to its advantages such as reduced converter rating, less acoustic noise, highly energy efficient and low power loss [7]. Substantial literature on DFIG based wind energy conversion system (WECS) both in standalone [8] and grid connected modes, is available [9]-[11]. In [8], the authors have presented DFIG based WECS operating in standalone with a battery energy storage (BES) connected directly at the DC link. Moreover, the comparative performance with and without BES is discussed. In [9], the authors have described an extended active power theory for effective operation of wind turbine coupled DFIG both in balanced and unbalanced grid conditions. Moreover, the DFIG is controlled with only rotor side converter (RSC). Therefore, the topology suffers from the power quality issues especially during harmonic loads. Liu *et al.* [10] have investigated the influence of phase locked loop parameters and grid strength on the stability of DFIG wind farm in grid connected mode. However, an experimental validation has not been performed. In [11], the authors have discussed a synchronization control method for smooth connection of DFIG to the grid. Moreover, it has been implemented on a modified IEEE 39 bus system using real time simulation platform. However, hardware realization has not been done. In other side, there has been increasing power generation through solar photovoltaic (PV) array worldwide. The solar energy conversion system (SECS) can be single stage or double stage. Some of the literature regarding solar PV system is reported in [12], [13]. Shah *et al.* [12] have demonstrated the single stage SECS connected to the utility grid. Moreover, a fundamental current extraction technique based on second-order generalized integrator with frequency-locked loop has been implemented for voltage source converter (VSC). In [13], the authors have presented the double stage SECS interacting to the grid. In addition, an adaptive algorithm of fast zero attracting normalized least mean fourth has been implemented for VSC to improve the power quality issues.

The operation of WECS and SECS separately, is not economical and reliable because of their intermittency. Therefore, the integration of both wind and solar sources, improves reliability of power generation [14], [15]. Morshed *et al.* [14] have presented wind-PV system with fault ride through

Sambasivaiah Puchalapalli is with the Department of Electrical Engineering, Indian Institute of Technology Delhi, New Delhi-110016, India (e-mail: sambasivaiah8888@gmail.com).

S. K. Tiwari is working with NTPC Ltd., Noida, Uttar Pradesh-201301, India (e-mail: shailendrakt@rediffmail.com).

Bhim Singh is with the Department of Electrical Engineering, Indian Institute of Technology Delhi, New Delhi-110016, India (e-mail: bsingh@ee.iitd.ac.in).

P.K. Goel is working with Ministry of Power, State Govt. of Goa, North Goa-403001, India (e-mail: pkgoel3866@yahoo.com).

This article has been accepted for publication in a future issue of this journal, but has not been fully edited. Content may change prior to final publication. Citation information: DOI 10.1109/TIA.2020.2999563, IEEE Transactions on Industry Applications

capabilities. In its topology, the solar PV array is connected at the DC link of DFIG based WECS through a boost converter and a DC-DC converter. However, it increases the switching losses and cost, because of additional DC-DC converter along with grid side converter. In [15], the authors have demonstrated the wind-solar PV system with BES in standalone mode. In its configuration, the solar PV array is connected at the DC link of wind turbine driven DFIG through a boost converter. However, the current through BES is not controlled, because it is directly connected at the DC link. Further, the microgrids based on DG, wind and solar sources have been developed and reported in the literature [16]-[18]. In [16], the authors have discussed the capacity planning of BES for a microgrid based on wind, solar and diesel sources that are located in island. However, optimal fuel operation of DG has not been discussed. In [17], the authors have demonstrated a wind-diesel microgrid for fuel efficient zone with BES. However, the BES current is not controlled due to its direct connection at the DC link. Moreover, the chances of getting away from fuel efficient zone is more due to connection of only one RE source. Venkatraman *et al.* [18] have presented a wind-solar-diesel microgrid with BES for certain remote area. However, the optimal operation of DG has been ignored while developing the source and load controllers. In any microgrid, the BES plays vital role during the mismatch of generation and demand. Moreover, it helps in extraction of maximum power both from wind and solar, especially when the generation is more than the demand. There are many maximum power point tracking (MPPT) techniques discussed in the literature, both for wind and solar to extract maximum power corresponding to particular wind speed and insolation, respectively [12], [13], [15], [19], [20].

This work presents a microgrid based on wind turbine driven DFIG, DG and solar PV array with BES, in order to minimize the fuel consumption of DG. In this, the DG is designed to deliver the base load requirement of a particular household locality. The main contributions of this study are on the control aspects of the scheme, which are as follows.

- A novel generalized concept is used to compute the reference DG power output for the DG to remain operating in optimal fuel consumption mode.
- The load side converter control (LSC) is designed to control DG along with the power quality issues such as load unbalance compensation, harmonics compensation and reactive power compensation.
- The RSC control is designed to extract maximum power from the wind turbine.
- The BES is connected to the common DC bus of back-back connected VSCs through a bidirectional buck/boost DC-DC converter. It aims to provide path for excess stator power of DFIG. Moreover, a solar PV array is directly connected at DC bus.
- The bidirectional buck/boost DC-DC converter control is designed in a way to extract maximum power from the solar PV array and to control the current through BES.
- A modified perturb and observe (P&O) MPPT algorithm is presented to obtain maximum power from a solar PV array.
- This microgrid configuration is implemented with minimum number of converters, thereby reducing the total system cost and switching losses.
- The DFIG stator currents and DG currents, are maintained balanced and sinusoidal, as per the IEEE 519 standard.

The wind-diesel-solar microgrid with BES, is modelled and simulated using SimPowerSystems tool box of MATLAB. The system performance is analyzed for variable wind speeds, variable insolation, effect on buck boost converter at varying loads and unbalanced nonlinear load connected at point of common coupling (PCC). To validate the microgrid operation, tests are performed on a developed prototype in the laboratory.

II. Configuration of Microgrid

The schematic configuration of the microgrid is depicted in Fig. 1. It consists of wind turbine, DFIG, DG, solar PV array, BES, bidirectional buck/boost DC-DC converter, RSC, LSC, interfacing inductors, Δ/Y transformer, linear and nonlinear loads, circuit breakers (CB_1 & CB_2), DC link capacitor and ripple filters etc. This microgrid is designed to deliver a peak load of 7.5 kW for a particular locality. The wind turbine generator and solar PV array, are designed to deliver a power of 7.5 kW each. In this scheme, the solar PV array is directly connected to DC link, whereas BES is connected through bidirectional buck/boost DC-DC converter. The DG is comprising of a synchronous generator of 4 pole, internal combustion engine of 4 stroke reciprocating type along with automatic voltage regulator (AVR). A 7.5 kVA DG is selected in line with rated capacity of the wind turbine generator. The design of a wind turbine generator, solar PV array, DG, BES and other components, is carried out based on the literature reported in [12], [15], [17]. Moreover, the design parameters of microgrid, are given in Appendices.

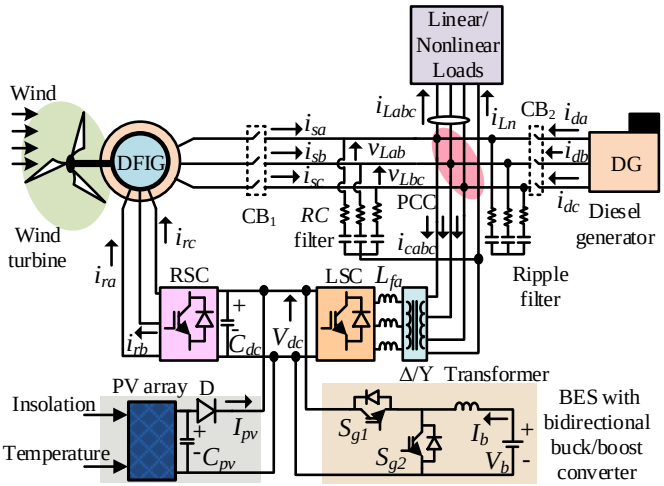

Fig. 1. DFIG based microgrid.

III. Control Algorithms of Microgrid

The complete description of control algorithms of RSC and LSC, MPPT algorithm of solar PV array, bidirectional buck/boost DC-DC converter, are given in following subsections.

A. Control Algorithm for RSC

The control algorithm of RSC, is depicted in Fig. 2. The RSC is used to supply the reactive power requirement of DFIG

This article has been accepted for publication in a future issue of this journal, but has not been fully edited. Content may change prior to final publication. Citation information: DOI 10.1109/TIA.2020.2999563, IEEE Transactions on Industry Applications

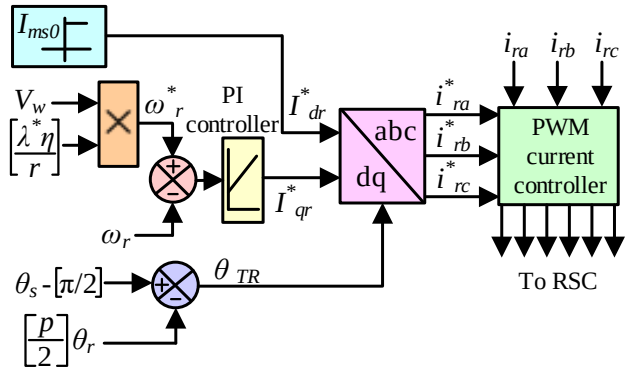

Fig. 2. RSC control algorithm.

and also to regulate the speed for achieving MPPT from the wind turbine. The field oriented vector control (FOVC) is used for RSC to generate the switching pulses, as shown in Fig. 2. In FOVC, direct axis and quadrature axis components of rotor currents (I^*_{dr}, I^*_{qr}) represent reactive and active components, respectively. The I^*_{dr} is corresponding to no load magnetizing current (I_{ms0}) of DFIG, which is computed as [21],

$$I_{ms0} = \frac{\sqrt{2}V_L}{\sqrt{3}X_m} \tag{1}$$

where X_m denotes the magnetizing reactance of the machine and V_L is the line voltage at the machine terminals.

The I^*_{qr} is estimated by passing the speed error through proportional and integral (PI) controller as depicted in Fig. 2 and it is derived as,

$$I^*_{qr(k)} = I^*_{qr(k-1)} + K_{p\omega}(\omega_{err(k)} - \omega_{err(k-1)}) + K_{i\omega}\omega_{err(k)} \tag{2}$$

where $K_{p\omega}$ and $K_{i\omega}$ represent proportional and integral constants of PI speed controller, respectively. The $\omega_{err(k)}$ and $\omega_{err(k-1)}$ denote speed error at kth and (k-1)th instants, respectively.

The $\omega_{err(k)}$, is obtained as,

$$\omega_{err(k)} = \omega^*_{r(k)} - \omega_{r(k)} \tag{3}$$

where $\omega^*_{r(k)}$ and $\omega_{r(k)}$ denote the reference and sensed rotor speed of DFIG at kth instant, respectively.

The reference rotor speed is obtained from the tip speed ratio MPPT control [19] as,

$$\omega^*_r = \eta\lambda^* V_w / r \tag{4}$$

where V_w, λ^*, η and r represent wind speed, optimal tip speed ratio, gear ratio and radius of wind turbine, respectively.

The rotor transformation angle (θ_{TR}) is computed as,

$$\theta_{TR} = \left(\theta_s - \frac{\pi}{2}\right) - \left(p/2\right)\theta_r \tag{5}$$

where θ_s is obtained from phase locked loop and θ_r is computed from the sensed rotor speed as,

$$\theta_r = \int_0^t (\omega_r) dt \tag{6}$$

Finally, reference rotor currents (i^*_{ra}, i^*_{rb} and i^*_{rc}) are derived from I^*_{qr} and I^*_{dr} using an angle of transformation θ_{TR}, as depicted in Fig. 2. These reference currents along with sensed rotor currents (i_{ra}, i_{rb} and i_{rc}), are applied to pulse width modulation (PWM) controller to produce RSC gating signals.

B. Control Algorithm for LSC

The LSC control algorithm is depicted in Fig. 3. The LSC is controlled to achieve the following objectives.

- It maintains the DG and DFIG stator currents sinusoidal and balanced.
- It regulates the DG power within the range of P_{Dmin} to P_{Dmax} to achieve optimal fuel consumption. Where P_{Dmin} and P_{Dmax} refer to minimum and maximum DG power output in pu for optimal fuel consumption.

A modified indirect vector control based on voltage oriented reference frame, is used to generate the reference currents as shown in Fig. 3. In this, both DG and DFIG stator currents are added and controlled to extract maximum power from the DFIG and to regulate the DG power within the range for optimal fuel consumption. The d-axis component of LSC is obtained as,

$$I^*_{dg} = I^*_{dd} + I^*_{dw} \tag{7}$$

where I^*_{dd}, I^*_{dw} denote the d-component current of DG and DFIG, respectively. It is noted that the saturation block is placed before the I^*_{dd} component to operate the DG in optimal fuel efficient zone at change in load, as depicted in Fig. 3.

In this work, a generalized concept is used to calculate the DG power based on state of the BES. The reference DG power in pu (P^*_D) is computed as,

$$P^*_D = P_{D\min} + k_1\beta \tag{8}$$

Here the value of β varies from 0 to 1. The minimum value of β is achieved when BES is charged to maximum voltage (V_{bmax}) whereas β takes maximum value when BES voltage falls to its minimum value (V_{bmin}). The β is of the form as,

$$\beta = \frac{V_{b\max} - V_b}{k_2} \tag{9}$$

In (8) and (9), k_1 and k_2 represent constant parameters. The value of k_1 is selected such that P^*_D attains its maximum limit of optimal fuel consumption as β tends to unity. Moreover, the value of k_2 is selected such that the β attains unity at V_{bmin}. In this work, the chosen values of P_{Dmin}, P_{Dmax}, V_{bmax}, V_{bmin}, k_1 and k_2 are mentioned in Appendices.

From (8), the I^*_{dd} is computed as,

$$I^*_{dd} = \left(\sqrt{2/3}\right) \times \left(\frac{P^*_D \times VA_{DG}}{V_L}\right) \tag{10}$$

where V_L and VA_{DG} represent line voltage at PCC and VA rating of DG, which is chosen as a base value.

The I^*_{dw} is computed as,

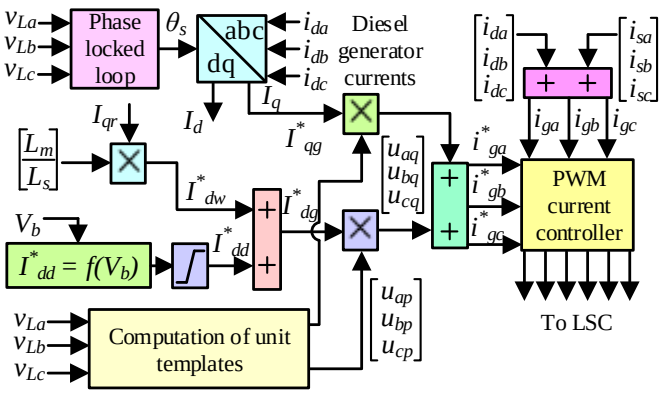

Fig. 3. LSC control algorithm.

$$I_{dw}^{*}=\left(\frac{L_m}{L_s}\right)I_{qr} \tag{11}$$

The DG currents (i_{da}, i_{db} and i_{dc}) are transformed to I_d and I_q using angle of transformation (θ_s), which is obtained from PLL as shown in Fig. 3. The q-axis component of LSC current (I^{*}_{qg}) is numerically same as I_q of DG. The I^{*}_{dg} and I^{*}_{qg} are multiplied with in-phase and quadrature unit templates, respectively and then added together to generate current references (i^{*}_{ga}, i^{*}_{gb} and i^{*}_{gc}). The unit templates are obtained from phase voltages (v_a, v_b and v_c), as shown in Fig. 3. Unit templates of in-phase components are obtained as,

$$\left.u_{ap}=\frac{v_a}{V_m},u_{bp}=\frac{v_b}{V_m},u_{cp}=\frac{v_c}{V_m}\right\} \tag{12}$$

where, V_m denotes the peak of phase voltage at PCC, which is computed as,

$$V_m=\{2(v_a^2+v_b^2+v_c^2)/3\}^{1/2} \tag{13}$$

The unit templates of quadrature components, are obtained from in-phase components as,

$$\left.\begin{aligned}u_{aq}&=-\frac{u_{bp}}{\sqrt{3}}+\frac{u_{cp}}{\sqrt{3}},u_{bq}=\frac{\sqrt{3}u_{ap}}{2}+\frac{u_{bp}-u_{cp}}{2\sqrt{3}},\\ u_{cq}&=-\frac{\sqrt{3}u_{ap}}{2}+\frac{u_{bp}-u_{cp}}{2\sqrt{3}}\end{aligned}\right\} \tag{14}$$

Finally, the generated reference currents and sensed currents (i_{ga}, i_{gb} and i_{gc}) are applied to PWM controller to produce pulses for LSC, as depicted in Fig. 3.

C. Solar PV Array MPPT Algorithm and Bidirectional Buck/Boost DC-DC Converter Control

The bidirectional buck or bidirectional boost DC-DC converter is used to regulate the DC link voltage by controlling power flow through the BES. By doing so, the solar MPPT is achieved. In this, a modified perturb and observe (P&O) algorithm is used, which consists of sampling pulse generation (X) and subsequently estimation of reference DC link voltage (V^{*}_{dc}) as depicted in Figs. 4-5, respectively. Fig. 4 illustrates various steps involved in the generation of sampling pulse 'X'. Here, the sampling pulse is a name

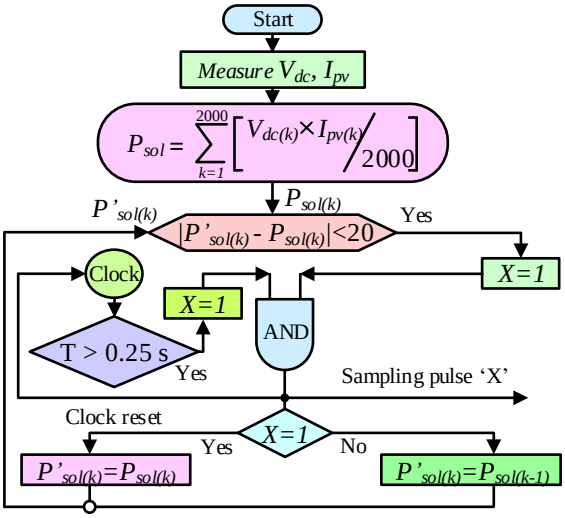

Fig. 4. Sampling pulse generation.

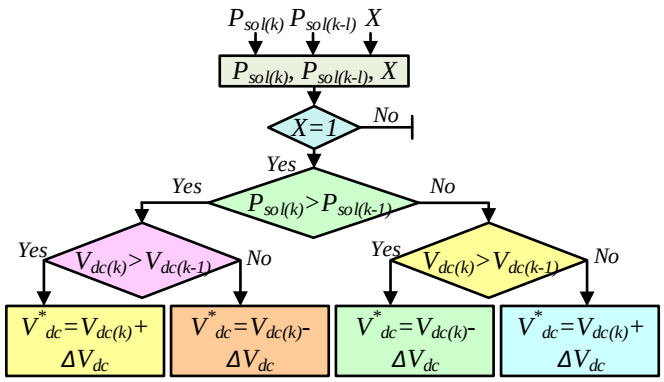

Fig. 5. MPPT algorithm of solar PV array.

given to variable 'X'. It varies between digital bits 0 and 1. In Fig. 4, the first step is to get the information of DC link voltage or solar PV voltage (V_{dc}) and solar PV current (I_{pv}) at kth instant and computation of instantaneous solar power. The second step is the determination of running average solar power (P_{sol}), which performs the same function as filtering. In case the absolute difference between the running averaged power (P_{sol}) and previously sampled power (P'_{sol}) is less than 20 W combined with minimum time delay of 0.25 s from previous sampling, the control senses that steady state has arrived. On sensing the steady state, the output of the sampling pulse 'X' becomes '1'. The sampling pulse decides the instant of incremental change in reference DC link voltage (V^{*}_{dc}) or solar PV MPPT voltage. The value of V^{*}_{dc} is updated only if sampling pulse becomes '1'. This is clearly evident from Fig. 5 that depicts the modified P&O MPPT algorithm. Once X becomes '1', the MPPT algorithm checks for $P_{sol(k)} > P_{sol(k-1)}$. If it is yes, then it again checks for $V_{dc(k)} > V_{dc(k-1)}$. If it is also yes, then, the new reference DC link voltage becomes $V^{*}_{dc} = V_{dc(k)} + \Delta V_{dc}$. Where ΔV_{dc} denotes the small incremental change in DC link voltage. The other scenarios are evident from the Fig. 5.

The bidirectional buck/boost DC-DC converter control, is demonstrated in Fig. 6. The outer proportional-integral (PI) controller of the bidirectional buck or bidirectional DC-DC boost converter control, is used to regulate the DC link voltage. Moreover, the output of the outer PI controller is reference battery current (I^{*}_{b}), as depicted in Fig. 6. The inner PI controller is used to track the reference battery current. Moreover, the output of the inner PI controller is the duty ratio (R) of the bidirectional buck/boost DC-DC converter. From Fig. 6, the reference battery current (I^{*}_{b}) is obtained as,

$$I^{*}_{b(k)}=I^{*}_{b(k-1)}+K_{pb}(V_{de(k)}-V_{de(k-1)})+K_{ib}V_{de(k)} \tag{15}$$

Where, error of the DC link voltage at kth instant is $V_{de(k)}=V^{*}_{dc(k)}-V_{dc(k)}$. Here $V^{*}_{dc(k)}$ and $V_{dc(k)}$ represent the reference DC link voltage and sensed DC link voltage at kth instant, respectively. K_{pb} and K_{ib} denote the proportional and

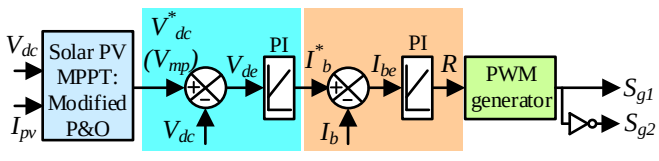

Fig. 6. Control of bidirectional buck or bidirectional boost converter.

integral constants of the outer PI controller.

Besides, the duty ratio (R) of the bidirectional DC-DC converter, is computed as,

$$R_{(k)} = R_{(k-1)} + K_{pr}(I_{be(k)} - I_{be(k-1)}) + K_{ir} I_{be(k)} \quad (16)$$

Where, error of the battery current at kth instant is $I_{be(k)} = I^{*}_{b(k)} - I_{b(k)}$. Here $I^{*}_{b(k)}$ and $I_{b(k)}$ represent the reference battery current and sensed battery current at kth instant, respectively.

The obtained duty ratio (R) is applied to PWM generator to produce pulses for the switches of the bidirectional buck or bidirectional boost converter.

IV. Simulation Results

The microgrid based on wind turbine driven DFIG, DG and solar PV array with BES, is simulated using MATLAB. Various signals used to analyze the system performance, are rms value of phase voltage (V_r), system frequency (f_L), DFIG rotor speed (ω_r), DG power (P_D), wind power from stator (P_w), solar PV power (P_{sol}), load power (P_L), LSC power (P_{LSC}), DC link voltage (V_{dc}), battery current (I_b), battery voltage (V_b), wind speed (V_w), insolation (G), rotor power coefficient (C_p), a-phase stator current (i_{sa}), rotor currents (i_{rabc}), a-phase DG current (i_{da}), a-phase PCC voltage (v_{La}), stator currents (i_{sabc}), DG currents (i_{dabc}), load currents (i_{La}, i_{Lb} and i_{Lc}), neutral current (i_{Ln}) and LSC currents (i_{cabc}). The parameters used for the simulation are mentioned in Appendices.

A. Performance of Bidirectional Buck/Boost DC-DC Converter at Change in Load

The performance of bidirectional buck or bidirectional boost DC-DC converter at change in the load, is depicted in Figs. 7 (a-b). The wind speed and insolation are kept at 7 m/s and 700 W/m^2, respectively. Initially a 3-phase balanced load of 2.5 kW is connected at PCC. The DG is delivering 4.84 kW (shown in Fig. 7 (b)), which corresponds to the battery bank voltage of 125 V. Moreover, the DFIG and solar PV array powers are 2.013 kW and 4.122 kW, respectively as depicted in Fig. 7 (b). Since the total generation is more than the local demand, the remaining power goes to BES through a bidirectional buck/boost DC-DC converter as shown in Fig. 7 (a). At t = 3 s, an additional load of 2 kW is connected and again it is disconnected at t = 5.5 s. During this period, it is observed that the power generation from all sources, remains unchanged and the increased load power is met by the BES through LSC. There is a minor sag and swell of DC link voltage, however, the solar MPPT is unaffected as seen from P_{sol} waveform. Moreover, the system voltage and frequency are maintained constant, as depicted in Fig. 7 (b).

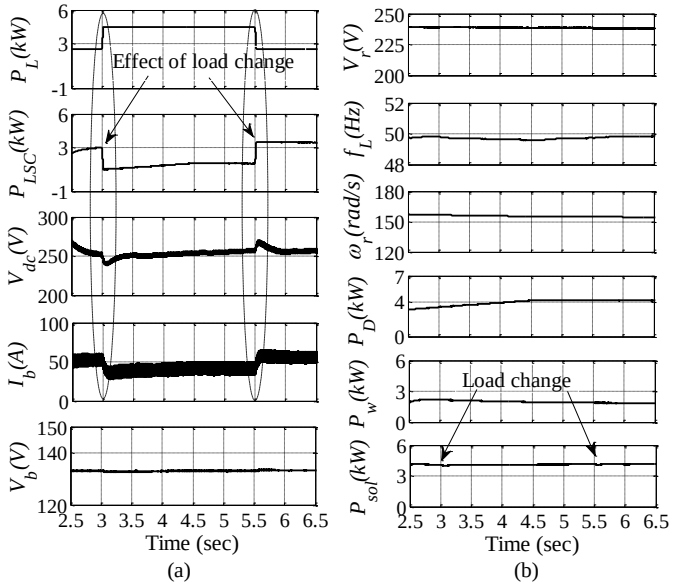

Fig. 7. (a-b) Performance of bidirectional buck/boost converter at change in load (a) P_L, P_{LSC}, V_{dc}, I_b and V_b (b) V_r, f_L, ω_r, P_D, P_w and P_{sol}.

B. System Performance at Variable Wind Speeds

The performance of the system at variable wind speeds are depicted in Figs. 8 (a-c). In this, a 3-phase load of 4 kW is connected at PCC and the insolation is kept at 700 W/m^2. The DG delivers power of 5.67 kW based on the state of the BES, as depicted in Fig. 8 (b). The pattern of wind speed variation is depicted in Fig. 8 (a). It is observed that the controller regulates the DFIG rotor speed as per wind MPPT algorithm, as depicted in Fig. 8 (a). Moreover, it is observed that the DC link voltage is regulated. The system dynamic response during the transition of DFIG speed from supersynchronous to subsynchronous speed region, is depicted in Fig. 8 (c). It is observed that wind MPPT is obtained during the variation of wind speed. Moreover, the frequency rotor currents, is changed according to the speed of operation of DFIG.

C. System Performance at Variable Insolation

The performance of the system at varying solar radiation, is depicted in Figs. 9 (a-b). In this, the wind speed is kept constant at 7 m/s. Moreover, the DG delivers 4.2 kW power based on the battery voltage, as depicted in Fig. 9 (b). In this, a 3-phase linear balanced load of nearly 4 kW is connected at PCC. The insolation of solar PV array is varied from 700 W/m^2 to 800 W/m^2 at t = 3 s and again it is reduced to 600 W/m^2 at t = 5.5 s, as depicted in Fig. 9 (a). The DC link voltage is regulated by the bidirectional DC-DC converter control for achieving the solar MPPT. Moreover, the solar MPPT is manifested by the P_{sol} waveform, as depicted in Fig. 9 (a).

D. System Performance at Unbalanced Nonlinear Load

The dynamic performance of the system at unbalanced nonlinear load, is depicted in Fig. 10. Initially, a balanced load of 6.7 kW is connected at PCC. It includes a linear load of 0.5 kW and remaining be the nonlinear load, connected on each phase. At t = 2.6 s, a-phase of the load is disconnected and subsequently phase-b, is also disconnected at t = 2.8 s, as depicted in Fig. 10. However, both voltages and currents of DFIG and DG, are maintained balanced and follow the IEEE 519 standard. The LSC helps in unbalance and harmonics compensation of the connected load at PCC. The LSC currents and neutral current, are also shown in Fig. 10. Moreover, the variation of power at unbalanced nonlinear load, is depicted in Fig. 11. Fig. 11 demonstrates waveforms of V_r, V_{dc}, I_b, P_{sol}, P_w, P_D, P_L and P_{LSC}. From these results, it is observed that the DC link voltage is regulated and moreover, solar PV and wind MPPT operation is unaffected. The decrease in load power goes to BES through LSC, which is evident from I_b, P_L and P_{LSC} waveforms. Moreover, V_r is maintained at constant value.

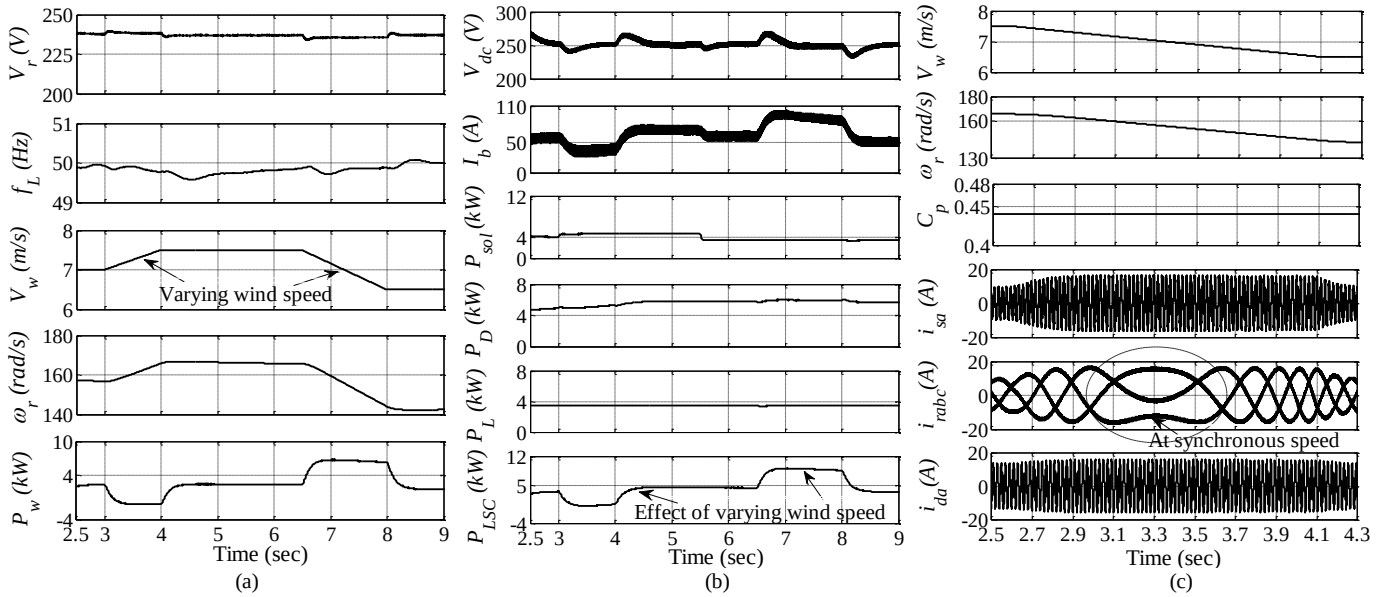

Fig. 8. System performance at variable wind speed (a) V_r, f_L, V_w, ω_r and P_w (b) V_{dc}, I_b, P_{sol}, P_D, P_L and P_{LSC}. (c) system performance during changeover of DFIG speed from supersynchronous to subsynchronous speed region: V_w, ω_r, C_p, i_{sa}, i_{rabc} and i_{da}.

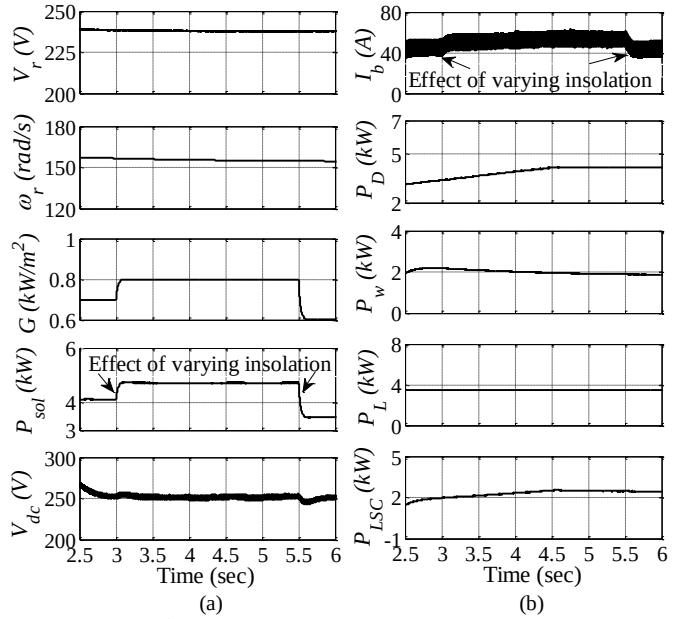

Fig. 9. System performance at variable insolation (a) V_r, ω_r, G, P_{sol} and V_{dc} (b) I_b, P_D, P_w, P_L and P_{LSC}.

V. Hardware Implementation of a Microgrid

An experimental prototype is developed in the laboratory to realize a wind-diesel-solar microgrid. A 3.7 kW wound rotor induction machine is used as DFIG. The separately excited DC motor and a buck chopper, are used to emulate the characteristics of a wind turbine. A V/F controlled induction motor-generator set is used as a DG. The solar PV simulator of a 5 kW capacity is used to realize the solar PV array. A battery bank of 20 numbers of 12 V, 7 Ah, are used to obtain the required voltage and kWh capacity. A bidirectional buck/boost DC-DC converter is used for the control of BES and to extract MPPT from the solar PV array. Moreover, two IGBT based 3-phase VSCs are used as LSC and RSC. The digital signal processor (dSPACE-1103) at a sampling time of 30 μs is used to implement the RSC and LSC control algorithms. The picture of the experimental prototype is depicted in Fig. 12. Moreover, the experimental parameters of the microgrid are given in Appendices.

A. System Performance at Varying Wind Speeds

The performance of microgrid at varying wind speeds and at constant insolation, is demonstrated in Figs. 13 (a-f). Fig. 13 (a) depicts waveforms of V_w, ω_r, i_{ra} and i_{da}. When the wind speed is increased, the rotor speed also increases as per the MPPT speed reference. In the similar way, the rotor speed decreases when the wind speed is decreased. The frequency of rotor current changes with change in wind speed. It is evident from i_{ra} that its frequency becomes DC exactly at synchronous speed of DFIG. However, the DG current remains constant as it depends on state of the battery and it is regulated by LSC. Fig. 13 (b) depicts waveforms of ω_r, i_{sa}, i_{ra} and P_s at varying wind speed. When the wind speed is increased, the stator power increases. Moreover, P_s decreases with a decrease in V_w. The stator current also increases and decreases, when the V_w is increased and decreased, respectively. Moreover, the variation of ω_r and i_{ra} with change in V_w, is apparent from Fig. 13 (b). Fig. 13 (c) depicts waveforms of i_{ra}, P_s, P_D and P_{LSC}. The wind speed is increased and decreased such that the DFIG speed changes between subsynchronous speed region to supersynchronous speed and vice versa. It is clearly evident from i_{ra} waveform. Since the load is kept constant, the increased stator power charges the BES through LSC. Therefore, the change in P_s due to change in V_w, is reflected in P_{LSC}. However, the DG power is regulated and it depends on state of the BES, in order to minimize the fuel consumption and to operate the DFIG in fuel efficient zone.

Fig. 13 (d) depicts waveforms of ω_r, i_{ra}, f_L and V_p at varying wind speeds. The waveforms ω_r and i_{ra} change with change in V_w. However, the system frequency and peak of phase voltage at PCC, are regulated at 50 Hz and 187.8 V, respectively. In addition, Fig. 13 (e) illustrates waveforms of P_s, P_{sol}, P_{LSC} and P_D. As V_w is increased, the stator power increases. Since the connected load is constant, the excess power goes to BES through LSC. It is clearly evident from

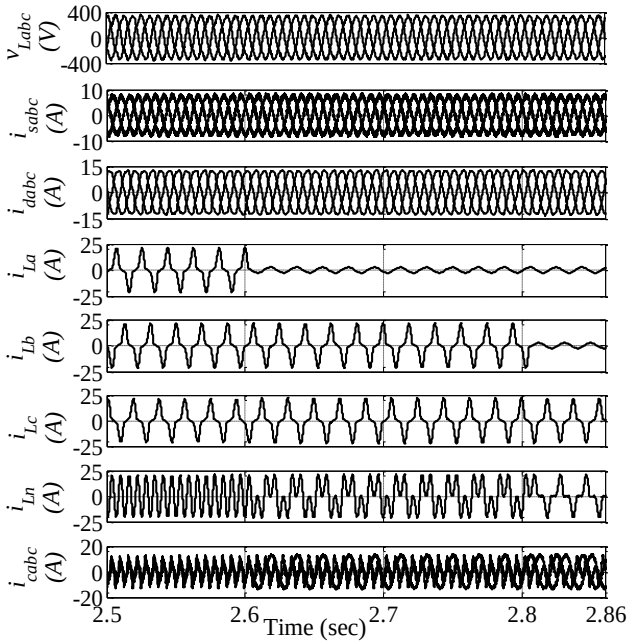

Fig. 10. System voltages and currents at unbalanced nonlinear load: v_{Labc}, i_{sabc}, i_{dabc}, i_{La}, i_{Lb}, i_{Lc}, i_{Ln} and i_{cabc}.

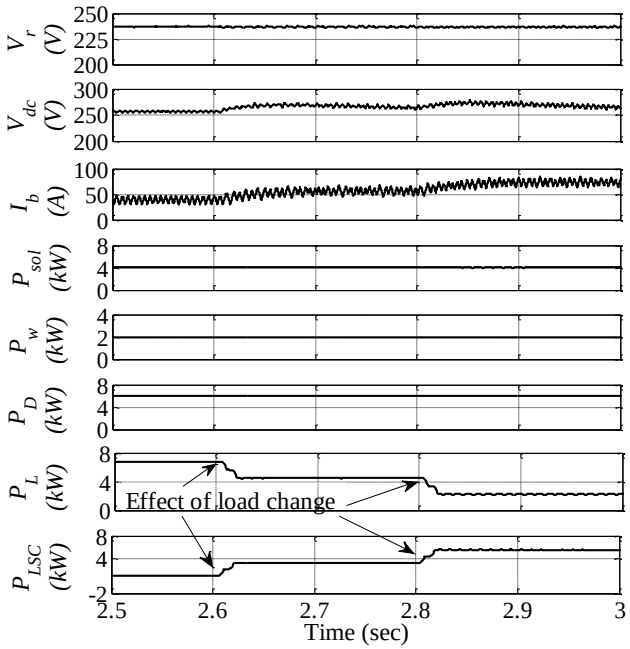

Fig. 11. System performance at nonlinear unbalanced load: V_r, V_{dc}, I_b, P_{sol}, P_w, P_D, P_L and P_{LSC}.

P_{LSC} waveform. Moreover, the generated power from solar PV array and DG, are constant. Fig. 13 (f) demonstrates waveforms of V_w, i_{ra}, V_{dc} and P_D. It is evident from these results that the DC link voltage is regulated by the bidirectional buck/boost DC-DC converter.

B. Performance of Microgrid at Load Change

The microgrid performance at sudden change in connected load is demonstrated in Figs. 14 (a-b). Fig. 14 (a) depicts waveforms of P_L, P_{LSC}, V_p and f_L at sudden disconnection and connection of 3-phase 3 wire load. The load power decreases and increases with disconnection and connection of the load, respectively. The decrease/increase in load power charges/discharges the BES, which is reflected in P_{LSC}.

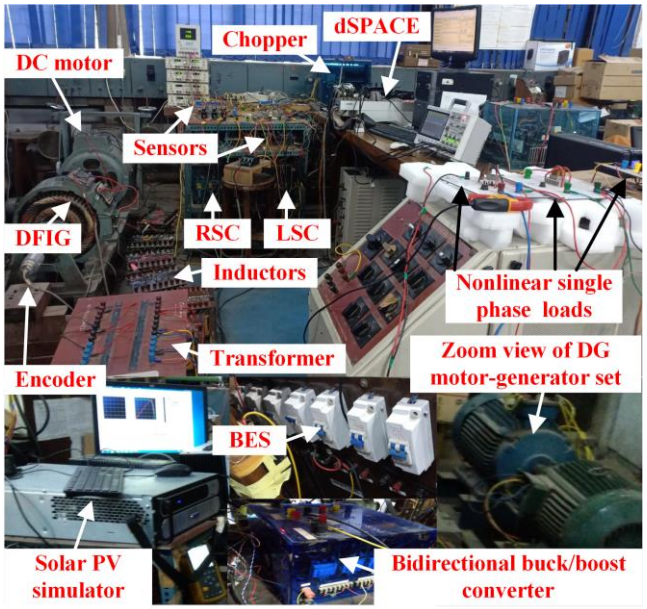

Fig. 12. Picture of the experimental prototype.

Moreover, the frequency and voltage at PCC, are maintained constant. It is to be noted that the PV insolation and wind speed are kept constant. In addition, Fig. 14 (b) depicts waveforms of v_{sa}, i_{La}, i_{ca} and i_{sa} at sudden disconnection of 3-phase nonlinear load at PCC. When the load is disconnected, the current through LSC (i_{ca}) increases, as it flows to BES. However, voltage and stator current are unaffected and sinusoidal. Moreover, Fig. 14 (c) demonstrates waveforms of v_{sa}, i_{La}, i_{ca} and i_{sa} at steady state, when a 3-phase diode bridge rectifier load is connected at PCC.

C. System Performance at 3-Phase 4 Wire Linear and Nonlinear Unbalanced Load

A 3-phase 4 wire, linear resistive load is connected at PCC. The steady state waveforms of three phase PCC voltages (v_{La}, v_{Lb} and v_{Lc}) and a-phase load current (i_{La}) is depicted in Fig. 15 (a) when the load in phase-a is suddenly disconnected. Fig. 15 (b) depicts the waveforms of v_{La}, neutral current (i_{Ln}), a-phase LSC current (i_{ca}) and a-phase load current (i_{La}) at linear load unbalancing. Initially, the connected load is balanced between each phase and neutral terminals and suddenly the load of phase-a, is disconnected to make the load unbalance. From Fig. 15 (b), it is noted that the neutral current is nearly zero when the load is balanced. However, the neutral current increases when the load is unbalanced. Moreover, the decreased load current flows to BES through LSC. Therefore, the LSC current also increases. Similarly, Figs. 15 (c-f) demonstrate system response when 3-phase 4 wire unbalanced nonlinear load is connected. From these results, it is evident that DG's voltages and currents are maintained balanced and sinusoidal, which is done effectively by the control of LSC.

D. Performance of Bidirectional Buck/Boost DC-DC Converter at Change in Solar PV Insolation

Figs. 16 (a-b) depict the waveforms of DC link voltage (V_{dc}), battery current (I_b), solar PV current (I_{pv}) and solar PV power (P_{sol}) at change in PV insolation. From Fig. 16 (a), when insolation is increased, the PV current and PV power are also increased. The increased current charges the BES, which is evident from I_b waveform. The bidirectional buck and

This article has been accepted for publication in a future issue of this journal, but has not been fully edited. Content may change prior to final publication. Citation information: DOI 10.1109/TIA.2020.2999563, IEEE Transactions on Industry Applications

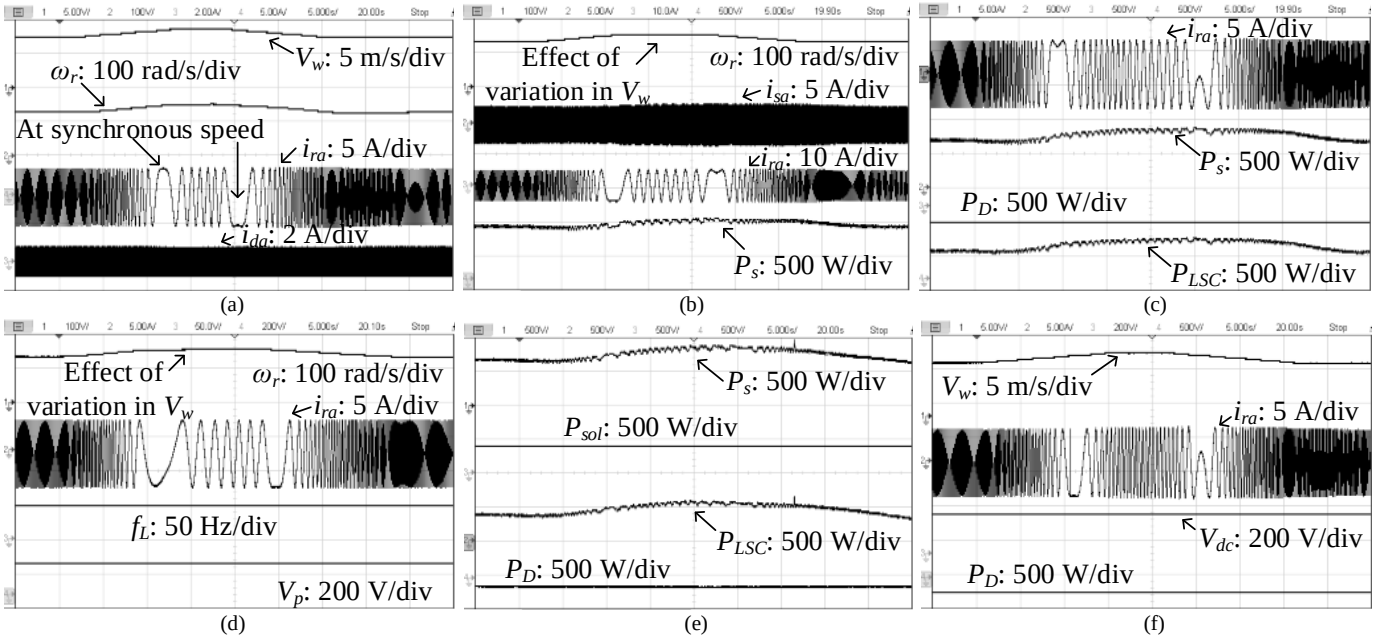

Fig. 13. System performance at varying wind speeds: (a) wind speed (V_w), rotor speed (ω_r), rotor current (i_{ra}) and DG current (i_{da}) (b) rotor speed (ω_r), stator current (i_{sa}), rotor current (i_{ra}) and stator power (P_s) (c) rotor current (i_{ra}), stator power (P_s), DG power (P_D) and LSC power (P_{LSC}) (d) rotor speed (ω_r), rotor current (i_{ra}), system frequency (f_L) and peak of phase voltage (V_p) (e) stator power (P_s), solar PV power (P_{sol}), LSC power (P_{LSC}) and DG power (P_D) (f) wind speed (V_w), rotor current (i_{ra}), DC link voltage (V_{dc}) and DG power (P_D).

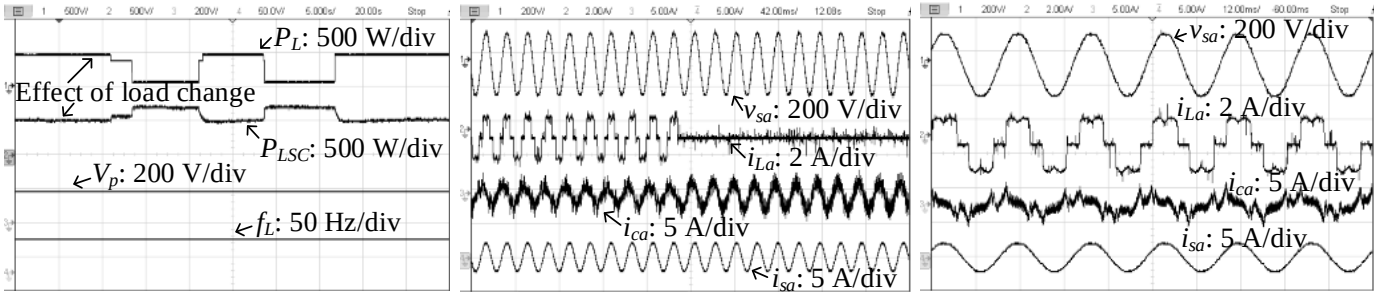

Fig. 14. System performance at 3-phase 3 wire load change: (a) load power (P_L), LSC power (P_{LSC}), peak of phase voltage (V_p) and system frequency (f_L) (b) DFIG stator voltage (v_{sa}), load current (i_{La}), LSC current (i_{ca}) and stator current (i_{sa}) (c) steady state performance at 3-phase nonlinear load.

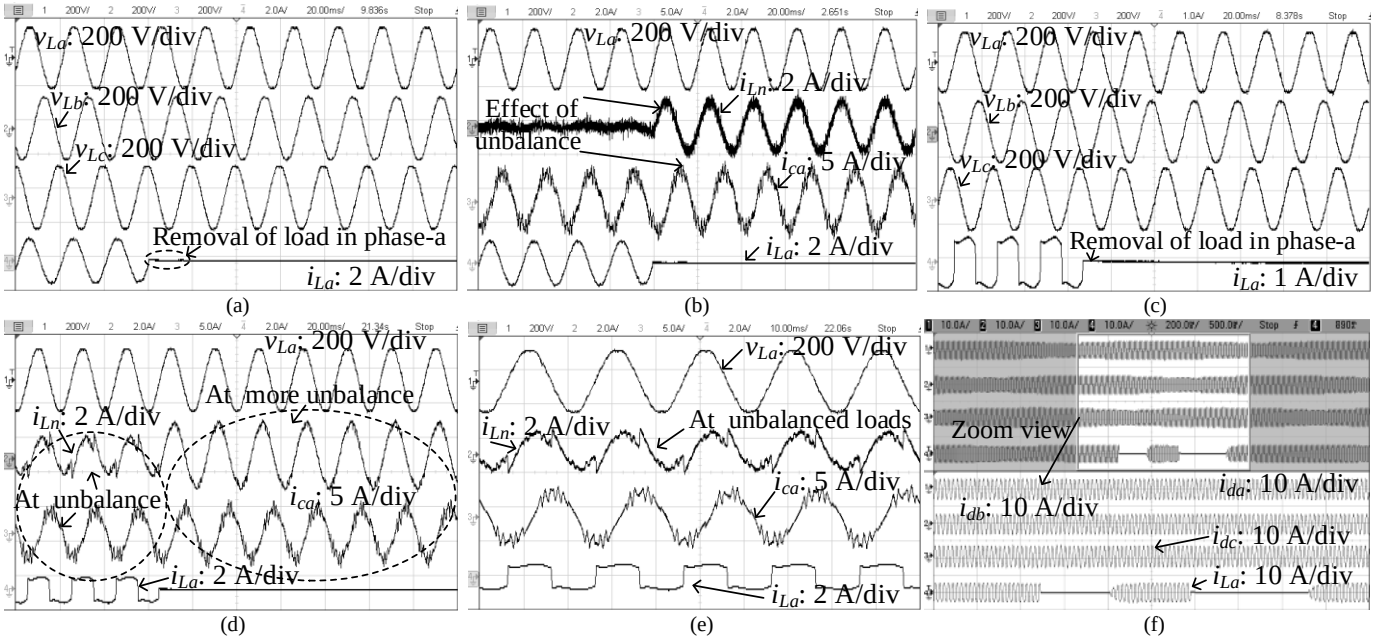

Fig. 15. (a-b) System performance at 3-phase 4 wire linear unbalanced load: (a) three-phase PCC voltages (v_{La}, v_{Lb} and v_{Lc}), a-phase load current (b) a-phase PCC voltage (v_{La}), neutral current (i_{Ln}), a-phase LSC current (i_{ca}), a-phase load current (i_{La}) (c-f) system performance at unbalanced nonlinear load: (c) v_{La}, v_{Lb} and v_{Lc} and i_{La} (d-e) v_{La}, i_{Ln}, i_{ca}, and i_{La} (f) diesel generator currents (i_{da}, i_{db} and i_{dc}) and a-phase load current (i_{La}).

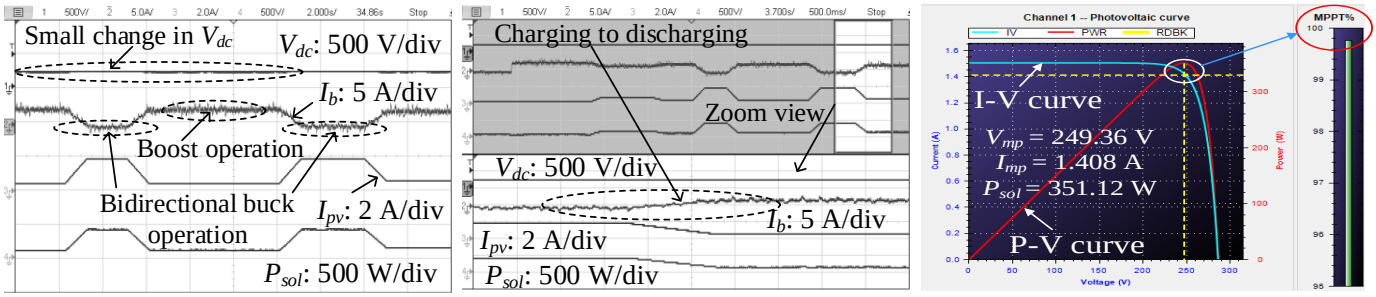

(a) (b) (c)

Fig. 16. Performance of the bidirectional buck/boost DC-DC converter at change in solar PV insolation (a-b) DC link voltage (V_{dc}), battery current (I_b), solar PV current (I_{pv}) and solar PV power (P_{sol}) (c) solar PV MPPT performance at insolation of 743 W/m^2.

bidirectional boost operation of the DC-DC converter, is clearly depicted in Fig. 16 (a). Moreover, the zoom view of BES charging to discharging transition when PV insolation is decreased, is demonstrated in Fig. 16 (b). In addition, solar PV MPPT performance at insolation of 743 W/m^2 is depicted in Fig. 16 (c). From Fig. 16 (c), it is apparent that the solar PV array MPPT is achieved close to 100%.

E. System Steady State Performance

Figs. 17 (a-b) show the steady state voltage and current waveforms of DFIG stator and DG, respectively. Moreover, the harmonic spectra of stator current and PCC voltage, are shown in Figs. 17 (c-d), respectively. From these results, it is noted that the total harmonic distortions (THDs) of both currents and voltages, are as per the IEEE 519 standard.

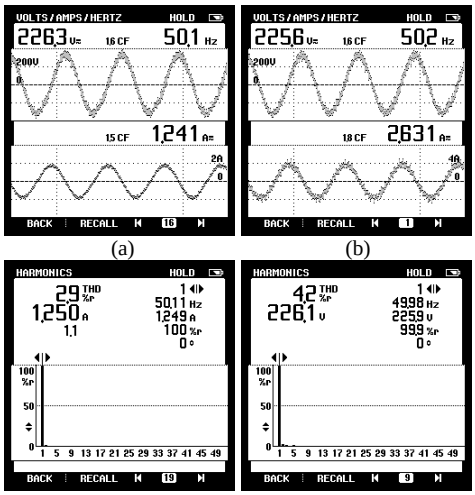

(a) (b) (c) (d)

Fig. 17. System steady state performance (a-b) voltage and current waveforms of DFIG stator and diesel generator (c-d) harmonic spectra of DFIG stator current and PCC voltage.

VI. Conclusion

The microgrid based on wind turbine driven DFIG, DG and solar PV array with BES, with minimum number of converters, has been presented. The solar PV array is directly connected to DC link of back-back connected VSCs, whereas BES is connected through a bidirectional buck/boost DC-DC converter. The system has been simulated for various scenarios such as variable wind speeds, variable insolation and unbalanced nonlinear load connected at PCC. Moreover, the performance of bidirectional buck/boost DC-DC converter at change in the load has been investigated. Simulated results have shown the satisfactory performance of the system to achieve optimal fuel consumption. The DFIG stator voltages, currents and DG currents, are found balanced and sinusoidal, as per the IEEE 519 standard. A prototype has been developed in the laboratory to validate the steady state and dynamic performances of the microgrid. Test results have shown quite good performance under variable wind speeds, linear and nonlinear unbalanced loads and at variable PV insolation.

Acknowledgments

The authors are grateful to Dept. of Science and Tech., Govt. of India (Grant Numbers: RP03443G (Indo-US Project), RP03391 (UKICERI)), J. C. Bose Fellowship (Grant Number: RP03128), and Fund for Improvement of Science and Technology (Grant Number: RP03195G (FIST)) for providing financial assistance to this work.

Appendices

A. Parameters of Simulation

DFIG: 7.5 kW, 415 V, 4 pole, 50 Hz, R_s=1.06 Ω, L_{ls} =81.62 mH, R_r =0.8 Ω, L_r =60.5 mH, L_s =206.5 mH, Inertia =1 kg-m^2; Wind turbine: Turbine rotor length, r=3.04 m, gear ratio η=11.79, λ^*=5.67, rotor power coefficient, C_p=0.441, rated wind speed=9 m/s, minimum and maximum rotor speeds of DFIG, ω_{rmin}=110 rad/s and ω_{rmax}=198 rad/s; Transformer: 12.5 kVA, 125/415 (delta/star); Solar PV array: array capacity of 7.5 kW, 240 V, module, V_{mp}=26.3, I_{mp}= 7.61 A, number of parallel strings N_p = 4, number of series modules in a string N_s = 10; Diesel generator: 7.5 kVA, 415 V, 4 pole, K_i of governor=4.15, K_p of governor=10, K_m=1, T_1=0.031s, fuel time constants of τ_2=0.1 s, τ_3=0.01 s, k_1=0.4, k_2=25, P^*_{Dmin}=0.65, P^*_{Dmax}=1.05; Battery energy storage (BES): V_{bnom}=132 V, V_{bmax}=144 V, V_{bmin}=119 V, 15.75 kWh, 1500 AH; value of boost inductor=2 mH; C_{dc}=10000 µF.

B. Experimental Parameters

DFIG: Make- McFEC Ltd, stator windings connection-Y, 4 pole, 50 Hz, 400 V, 3.7 kW, Inertia=0.1878 kg-m^2, L_{lr}=6.832 mH, L_{ls}=6.832 mH, L_m=219 mH, R_r=1.708 Ω, R_s=1.32 Ω; DC motor of 230 V, 5 kW, R_f = 220 Ω, R_a = 1.3 Ω, L_f = 7.5 H, L_a =7.2 mH, K_ϕ=1.3314; Diesel generator (Induction machine): 230 V, 3.7 kW, 50 Hz, L_{ls}=2.01 mH, R_s=0.3939 Ω, L_{lr}=2.5 mH, R_r=0.4791 Ω, J=0.0011 kg-m^2, L_m=35.4 mH, Δ/Y transformer of 230/400, 10 kVA; solar PV array capacity of 5 kW, 240 V, 3 A; BES: 20 units, 12 V, 7 AH; Interfacing inductor=1.2 mH, Ripple filter of 5 Ω, 10 µF.

REFERENCES

[1] J. Knudsen, J. D. Bendtsen, P. Andersen, K. K. Madsen, and C. H. Sterregaard, "Supervisory control implementation on diesel-driven generator sets," *IEEE Trans. Ind. Electron.*, vol. 65, no. 12, pp. 9698-9705, Dec. 2018.

[2] J. Jo, H. An, and H. Cha, "Stability improvement of current control by voltage feedforward considering a large synchronous inductance of a diesel generator," *IEEE Trans. Ind. Applicat.*, vol. 54, no. 5, pp. 5134-5142, Sept.-Oct. 2018.

[3] Y. Zhang, A. M. Melin, S. M. Djouadi, M. M. Olama and K. Tomsovic, "Provision for guaranteed inertial response in diesel-wind systems via model reference control," *IEEE Trans. Power Systems*, vol. 33, no. 6, pp. 6557-6568, Nov. 2018.

[4] N. Nguyen-Hong, H. Nguyen-Duc, and Y. Nakanishi, "Optimal sizing of energy storage devices in isolated wind-diesel systems considering load growth uncertainty," *IEEE Trans. Ind. Applicat.*, vol. 54, no. 3, pp. 1983-1991, May-June 2018.

[5] W. Li, P. Chao, X. Liang, J. Ma, D. Xu, and X. Jin, "A practical equivalent method for DFIG wind farms," *IEEE Trans. Sustain. Energy*, vol. 9, no. 2, pp. 610-620, April 2018.

[6] T. Adefarati, R. C. Bansal, and J. John Justo, "Techno-economic analysis of a PV–wind–battery–diesel standalone power system in a remote area," *The Journal of Engineering*, vol. 2017, no. 13, pp. 740-744, 2017.

[7] C. Wu and H. Nian, "Stator harmonic currents suppression for DFIG based on feed-forward regulator under distorted grid voltage," *IEEE Trans. Power Electron*., vol. 33, no. 2, pp. 1211-1224, Feb. 2018.

[8] N. K. Swami Naidu and B. Singh, "Experimental implementation of doubly fed induction generator-based standalone wind energy conversion system," *IEEE Trans. Ind. Applicat.*, vol. 52, no. 4, pp. 3332-3339, July-Aug. 2016.

[9] D. Sun, X. Wang, H. Nian, and Z. Q. Zhu, "A sliding-mode direct power control strategy for DFIG under both balanced and unbalanced grid conditions using extended active power," *IEEE Trans. Power Electron.*, vol. 33, no. 2, pp. 1313-1322, Feb. 2018.

[10] Ju Liu, Wei Yao, Jinyu Wen, Jiakun Fang, Lin Jiang, Haibo He, and Shijie Cheng, "Impact of power grid strength and PLL parameters on stability of grid-connected DFIG wind farm," *IEEE Trans. Sustain. Energy*, vol. 11, no. 1, pp. 545-557, Jan. 2020.

[11] A. Thakallapelli, S. Kamalasadan, K. M. Muttaqi, and M. T. Hagh, "A synchronization control technique for soft connection of doubly fed induction generator based wind turbines to the power grids," *IEEE Trans. Ind. Applicat.*, vol. 55, no. 5, pp. 5277-5288, Sept.-Oct. 2019.

[12] P. Shah, I. Hussain, and B. Singh, "Single-stage SECS interfaced with grid using ISOGI-FLL-based control algorithm," *IEEE Trans. Ind. Applicat.*, vol. 55, no. 1, pp. 701-711, Jan.-Feb. 2019.

[13] A. K. Singh, I. Hussain, and B. Singh, "Double-stage three-phase grid-integrated solar PV system with fast zero attracting normalized least mean fourth based adaptive control," *IEEE Trans. Ind. Electron.*, vol. 65 , no. 5, pp. 3921-3931, May 2018.

[14] M. J. Morshed and A. Fekih, "A novel fault ride through scheme for hybrid wind/PV power generation systems," *IEEE Trans. Sustainable Energy*, Early Access.

[15] S. K. Tiwari, B. Singh, and P. K. Goel, "Design and control of autonomous wind–solar system with DFIG feeding 3-phase 4-wire loads," *IEEE Trans. Ind. Applicat.*, vol. 54, no. 2, pp. 1119-1127, March-April 2018.

[16] Y. Zhang, J. Wang, A. Berizzi, and X. Cao, "Life cycle planning of battery energy storage system in off-grid wind–solar–diesel microgrid," *IET Gener., Trans. & Distr.*, vol. 12, no. 20, pp. 4451-4461, Nov. 2018.

[17] S. K. Tiwari, B. Singh, and P. K. Goel, "Control of wind–diesel hybrid system with BESS for optimal operation," *IEEE Trans. Ind. Applicat.*, vol. 55, no. 2, pp. 1863-1872, March-April 2019.

[18] K. Venkatraman, B. Dastagiri Reddy, M. P. Selvan, S. Moorthi, N. Kumaresan, and N. A. Gounden, "Online condition monitoring and power management system for standalone micro-grid using FPGAs," *IET Gener., Trans. & Distr.*, vol. 10, no. 15, pp. 3875-3884, Nov. 2016.

[19] S. Puchalapalli and B. Singh, "A single input variable FLC for DFIG-based WPGS in standalone mode," *IEEE Trans. Sustainable Energy*, vol. 11, no. 2, pp. 595-607, April 2020.

[20] J. Hussain and M. K. Mishra, "Adaptive maximum power point tracking control algorithm for wind energy conversion systems," *IEEE Trans. Energy Convers.*, vol. 31, no. 2, pp. 697-705, June 2016.

[21] S. Puchalapalli, S. K. Tiwari, B. Singh, and P. K. Goel, "A microgrid based on wind driven DFIG, DG and solar PV array for optimal fuel consumption," in *8th IEEE Power India International Conference (PIICON)*, Kurukshetra, India, 2018, pp. 1-6.

Sambasivaiah Puchalapalli (S'16, M'19) was born in SPSR Nellore, Andhra Pradesh, India, in 1992. He received the B.Tech. degree in electrical and electronics engineering from N.B.K.R. Institute of Science and Technology, Vidyanagar, Andhra Pradesh, India, in 2013, and the M.Tech. degree in electrical engineering from IIT Gandhinagar (Recipient of the Institute Gold Medal), Gujarat, India, in 2016. He is currently working toward the Ph.D. degree in the Department of Electrical Engineering, IIT Delhi, New Delhi, India. His research interests include doubly fed induction generator-based wind energy conversion systems, and microgrid-based power systems.

Shailendra Kumar Tiwari received his B.E. (Electrical) from Govt. Engineering College, Raipur (Now NIT Raipur) India, in 1996. In 1997 he joined NTPC Ltd as Engineer, Power Plant Commissioining. In 2007, he did his M. Tech. (Power Generation Technology) from IIT Delhi, through company sponsered programme. In 2018, he completed his Ph.D. from IIT-Delhi. Presently, he is working as Additional General Manager in its Renewable Engineering Department of NTPC Ltd, at Noida, Near New Delhi. His area of research include solar and wind energy conversion, solar energy estimation.

Bhim Singh (SM'99, F'10) was born in Rahamapur, Bijnor (UP), India, in 1956. He has received his B.E. (Electrical) from the University of Roorkee (Now IIT Roorkee), India, in 1977 and his M.Tech. (Power Apparatus & Systems) and Ph.D. from the IIT Delhi, India, in 1979 and 1983, respectively. In 1983, he joined the Department of Electrical Engineering, University of Roorkee, as a Lecturer. He became a Reader there in 1988. In December 1990, he joined the Department of Electrical Engineering, IIT Delhi, India, as an Assistant Professor, where he has become an Associate Professor in 1994 and a Professor in 1997. He has been Head of the Department of Electrical Engineering at IIT Delhi from July 2014 to August 2016. He has been Dean, Academics at IIT Delhi , August 2016 to August 2019. He is JC Bose Fellow of DST, Government of India since December 2015. He is CEA Chair Professor since January 2019. Prof. Singh has guided 84 Ph.D. dissertations, and 167 M.E./M.Tech./M.S.(R) theses. He has been filed 56 patents. He has executed more than eighty sponsored and consultancy projects. His areas of interest include solar PV grid interface systems, microgrids, power quality monitoring and mitigation, solar PV water pumping systems, improved power quality AC-DC converters.

Puneet Kumar Goel was born in New Delhi, India, in 1966. He completed B. Tech in Electrical Engineering from IIT-Kanpur, India, in 1987, M. Tech. in Power Apparatus & Systems from IIT-Delhi, India in 1989, M.S. in Electrical Engineering from U.S.C., Los Angeles, USA in 2001 and Ph.D. from IIT-Delhi, India in 2009. In 1991, he joined Indian Administrative Service, where his assignments include Secretary (Power), Andaman & Nicobar Islands, India; Director (Thermal), Ministry of Power, Govt. of India; Executive Director, Rural Electrification Corporation of India Limited; Chairman and Managing Director, Delhi Transco and Secretary (Power), Govt. of NCT of Delhi, Commissioner, South Delhi Municipal Corporation, New Delhi. Presently, he is Principal Secretary (Power and Renewable Energy), Govt. of Goa, India. In 2017, he received National Energy Conservation Award from President of India. His areas of interest include solar PV grid interface systems, renewable energy sources, micro-grids, power electronics and electrical machines.